Article

A Static Stability Analysis Method for Passively Stabilized Sounding Rockets

Riccardo Cadamuro †, Maria Teresa Cazzola *,†, Nicolò Lontani † and Carlo E. D. Riboldi *

Department of Aerospace Science and Technology, Politecnico di Milano, Via La Masa 34, 20156 Milano, Italy; riccardo.cadamuro@mail.polimi.it (R.C.); nicolo1.lontani@mail.polimi.it (N.L.)

* Correspondence: mariateresa.cazzola@mail.polimi.it (M.T.C.); carlo.riboldi@polimi.it (C.E.D.R.)

† These authors contributed equally to this work.

Abstract: Sounding rockets constitute a class of rocket with a generally simple layout, being composed of a cylindrical center-body, a nosecone, a number of fins placed symmetrically around the longitudinal axis (usually three or four), and possibly a boat-tail. This type of flying craft is typically not actively controlled; instead, a passive stabilization effect is obtained through suitable positioning and sizing of the fins. Therefore, in the context of dynamic performance analysis, the margin of static stability is an index of primary interest. However, the classical approach to static stability analysis, which consists in splitting computations in two decoupled domains, namely, around the pitch and yaw axis, provides a very limited insight to the missile performance for this type of vehicle due to the violation of the classical assumptions of planar symmetry and symmetric flight conditions commonly adopted for winged aircraft. To tackle this issue, this paper introduces a method for analyzing static stability through a novel index, capable of more generally assessing the level of static stability for sounding rockets, exploiting the same information on aerodynamic coefficients typically required for more usual (i.e., decoupled) static stability analyses, and suggests a way to assess the validity and shortcoming of the method in each case at hand.

1. Introduction

Sounding rockets constitute a class of rockets often employed to carry out scientific observations and perform experiments in the higher layers of the atmosphere, or when experiencing a field of motion featuring high acceleration intensity is of interest (for example, for testing novel sensors). Their layout is usually simple, being composed of a cylindrical center-body, a nosecone, a number of fins placed symmetrically around the longitudinal axis (usually three or four), and possibly a boat-tail. Fins are usually sized to achieve certain performances in terms of passive stabilization. An object is considered passively stabilized if it does not present any control system that modifies its stability or trajectory during flight. Whenever an angle of attack develops during the flight of the rocket, the fins on the back generate a force responsible for the stabilizing moment, contributing to the balance around the center of mass. Another way to achieve passive stabilization is through the gyroscopic effect by making the object spin around its lower moment of inertia axis, a technique used in the majority of firearm projectiles that is beyond the scope of this paper. When it comes to assessing the level of stability, most of the existing literature concentrates on the results obtained from a standard analysis, usually carried out according to methods originally developed for winged aircraft.

The definition of longitudinal and directional static stability, typically introduced for flying bodies featuring a vertical plane of symmetry (i.e., most winged aircraft) [1–3], has

been applied to rockets in papers and books. For example, Fleeman [4] explains how the usual static stability criterion based on a sign constraint applied to a stability derivative (recalled in Section 2 in this text) holds also for missiles. Several practical applications [5–7] instead take advantage of Barrowman's formulation [8] to compute the center of pressure position, as well as the static stability margin, through a specific procedure. However, none of them takes into account lateral-directional stability explicitly.

Even when actively controlled missiles are of interest, the investigation of control laws to enhance the level of static (or dynamic) stability is typically carried out by splitting the longitudinal and lateral-directional domains and considering them as uncoupled [9,10].

This approach to static stability analysis is intrinsically limited in scope, since it neglects the change in the overall setup of aerodynamic forces and moments on the body due to the actual direction of the perturbation.

Another assumption often made is that there is no relation between the components of the aerodynamic moment and the aerodynamic angles defined with respect to two different planes [11], or in analytic terms, the stability derivatives of the pitching moment with respect to side-slip ($c_{m_{CG_\beta}}$) and of the yawing moment with respect to the angle of attack ($c_{n_{CG_\alpha}}$) are considered null. Though this assumption is justified for a classically configured winged aircraft, it is not necessarily verified for the geometry and flight characteristics of rockets instead. The adoption of that hypothesis affects how well the two usual static margins (i.e., longitudinal and directional) alone are capable of describing the static stability qualities.

Therefore, for the rockets which are the subject of this study, static stability indices are parameters of great relevance, both for prediction at the design stage and for verification in the field. In fact, only a configuration offering an acceptable level of static stability on its own (i.e., without stability-augmentation systems) can be adopted for a successful sounding rocket flight. In this context, the employment of the traditional decoupled analysis to the typical configuration of sounding rockets (i.e., cylindrical center body, nosecone, and fins placed symmetrically around the longitudinal axis) can lead to misleading, and sometimes even dangerous, results. A given configuration could be predicted as either stable or unstable by simply changing the reference frame in which the computations are performed. Moreover, the presence of numerical singularities when evaluating specific flight conditions, as will be investigated in Section 2, proves the classical formulation to be unreliable in a generic flight condition.

Section 2 presents the classical static stability analysis theory and how it is applied to rockets, in particular, highlighting its limits and shortcomings when applied to passively stabilized rockets. The cases of a three- and four-finned rocket, based on a test-bed geometry, will be analyzed. In Section 3, we provide and justify the equations to compute the new compounded stability index, as well as suggesting a way to determine the validity of that index in each case considered.

Section 4 shows the numerical results of both the new and the classical methodologies in a realistic test case. Finally, the static stability analysis method proposed herein was successfully applied to the design of a sounding rocket test-bed in the field, called *Gemini*. Details of this application are discussed in Section 5. The conclusions are then presented in Section 6.

The evaluation of aerodynamic quantities required for assigning a virtual model of the rocket was carried out through `Missile DATCOM 97` [12,13], and the results cross-checked through CFD simulations, as shown in Appendix A.

2. Classical Static Stability Analysis Applied to Missiles

In the literature dedicated to flight dynamics, when it comes to evaluating the static stability of an aircraft, it is typical to discuss the levels of longitudinal and lateral-directional static stability [2,3]. An aircraft is said to be statically stable in the longitudinal plane when the derivative with respect to the angle of attack α of the pitching moment coefficient in the center of gravity $\boldsymbol{CG}$, $C_{m_{CG}}$ is negative, yielding the well-known criterion

$$c_{m_{CG_\alpha}} < 0. \tag{1}$$

For a rocket, the longitudinal static margin is an index of the intensity of the system static response to a perturbation and is defined as SM_{lon}, according to Equation (2)

$$SM_{lon} = \frac{c_{m_{CG}}}{c_N}, \tag{2}$$

where c_N is the force coefficient in the direction of the body axis z^B, as in Figure 1 (note that the reference frame and sign conventions are adopted according to the `Missile DATCOM 97` user's manual [12] and may differ from the more standard nomenclature adopted for winged aircraft).
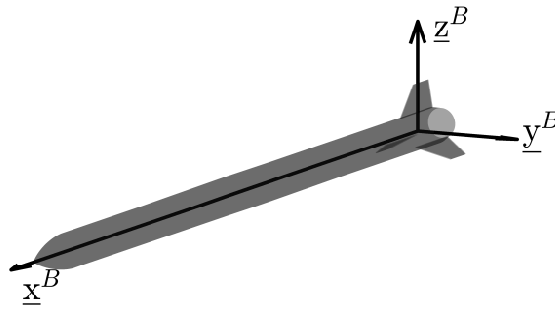

Figure 1. Rocket body reference frame.

Considering the lateral-directional motion, the aircraft is said to be statically stable in a directional sense when the derivative of the yawing moment $c_{n_{CG}}$ with respect to the sideslip angle β is positive, yielding the criterion

$$c_{n_{CG_\beta}} > 0, \tag{3}$$

and the directional static margin for a rocket is defined correspondingly as

$$SM_{dir} = -\frac{c_{n_{CG}}}{c_Y}, \tag{4}$$

where c_Y is a side force coefficient, proportional to the aerodynamic force component along y^B in Figure 1. In Equation (4), a negative sign is included in the definition, so that both the static margins SM_{lon} and SM_{dir} are positive for a stable condition.

2.1. Limits of the Classical Formulation

This section aims at investigating the limits of the classical formulation for static stability assessment when it is applied to certain geometries, specifically those with aerodynamic surfaces not aligned with any axes of the body reference system, which are of great relevance for sounding rockets. To ensure a comprehensive analysis, the cases of a four-finned and a three-finned configuration will both be analyzed.

To introduce the following discussion, consider that a longitudinal stability analysis is typically employed in the rocket design loop as a component of performance assessment, and is of particular interest when the rocket is flying in a typical symmetric condition with a null roll angle ϕ (see Figure 2).
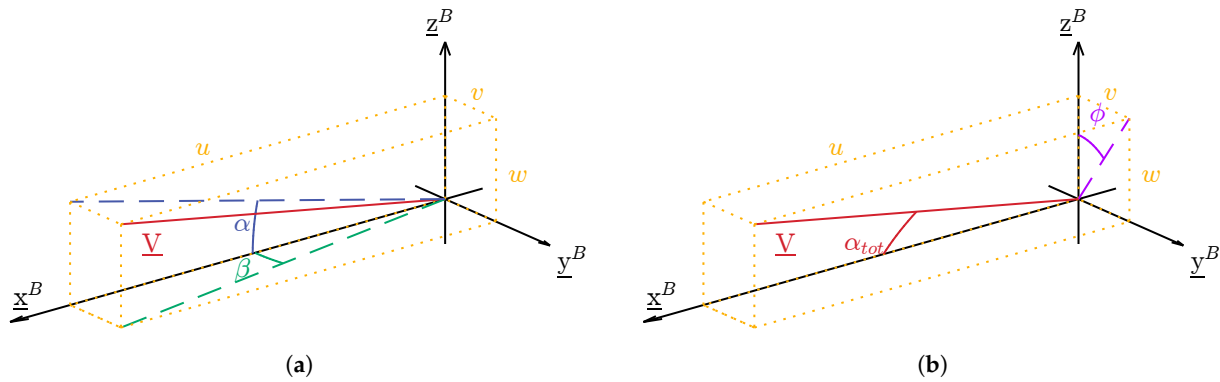
(**a**)   (**b**)

Figure 2. Two sets of equivalent aerodynamic angles to describe the direction of a perturbation. (**a**) α and β. (**b**) α_{tot} and ϕ.

The left plot in Figure 2 shows the definitions of the angle of attack α and the sideslip angle β for a missile associated to the body frame $(\cdot)^B$. On the right plot, the same missile and flight condition are described via a total angle of attack α_{tot}. In the latter case, the aerodynamic roll angle ϕ has been introduced in association to a plane obtained from the original body plane normal to y^B, rotating it around the longitudinal axis x^B, so as to have the velocity vector lying on the new plane.

Considering now a condition where $\phi \neq 0$ (right plot), it can be observed that in contrast to a purely symmetric flight case, the lateral-directional dynamics will be directly involved in the stability analysis when α_{tot} is figuratively perturbed. Therefore, in that case, considering only the longitudinal behavior may be expected to produce inaccuracies in estimating the static stability margin.

2.1.1. Four-Finned Rocket

Consider evaluating both the classical static margins in Equations (2) and (4) for a rocket with four equal fins, arranged in a radial configuration, repeating the analysis for a varying value of the aerodynamic angle ϕ. The body reference frame is the one considered in Figure 1.

Figure 3 shows the two static margins as a function of the aerodynamic roll angle ϕ considering constant values of the total angle of attack α_{tot} and Mach number ($\alpha_{tot} = 15°$ and $M = 0.1$; the aerodynamic coefficients are computed through `Missile DATCOM 97` [12]). These conditions are of interest since they are encountered at launchpad exit with a wind magnitude at 9 m/s and a launchpad elevation of 90°.
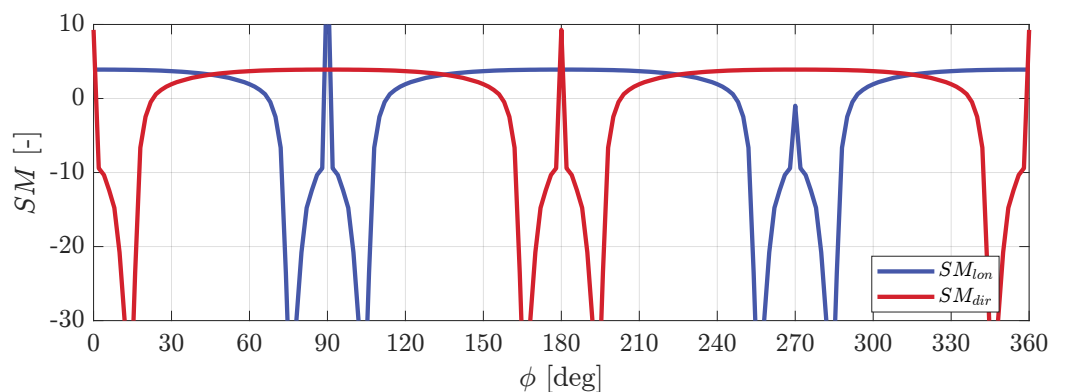

Figure 3. Longitudinal and directional static margins as functions of the aerodynamic roll angle ϕ for a four-finned rocket.

The two static margins feature asymptotes, where the respective force values (and the corresponding moment) tend to zero. In particular, regarding the longitudinal static

stability, C_N is null at ϕ equal to $90°$ or $270°$, whereas for lateral static stability, C_Y is null where ϕ is equal to $0°$ or $180°$.

It should be pointed out that choosing the body reference frame orientation with respect to the body is not as straightforward as it is for standard winged aircraft due to the fins being arranged in a radial symmetry. Considering again the same four-finned rocket and flight condition, Table 1 reports the longitudinal and directional static margins for a single flight condition, evaluated in different reference systems, where the longitudinal plane of the body, normal to y^B, and the corresponding reference system, is aligned with a different fin.

Table 1. Longitudinal and directional static margin at $\alpha_{tot} = 15°$ with respect to different body reference frames (reflected by different values of ϕ), each with the z^b axis aligned with respect to a different fin in a four-finned configuration.

Reference Frame	SM_{lon}	SM_{dir}	ϕ
$\mathcal{RF}_1$	3.86	-23.56	$16°$
$\mathcal{RF}_2$	-23.56	3.86	$106°$
$\mathcal{RF}_3$	3.86	-23.56	$196°$
$\mathcal{RF}_4$	-23.56	3.86	$286°$

As can be expected, from Table 1, it is possible to note that for a four-finned rocket, the results depend on the actual body reference adopted according to a periodic rule. In particular, the values of the longitudinal and the directional static margins are repeated every $90°$.

In order to further interpret these results through the crossed derivatives $c_{m_{CG_\beta}}$ and $c_{n_{CG_\alpha}}$ mentioned in Section 1, it can be reported that for the same four-finned rocket these quantities are null, in particular, for all the considered body references in Table 1. Therefore, the longitudinal and directional static margins are not coupled in this configuration.

These derivatives were checked numerically for changing values of β (for $c_{m_{CG_\beta}}$) and α (for $c_{n_{CG_\alpha}}$) and are presented in Figure 4, clearly showing their constantly negligible value.
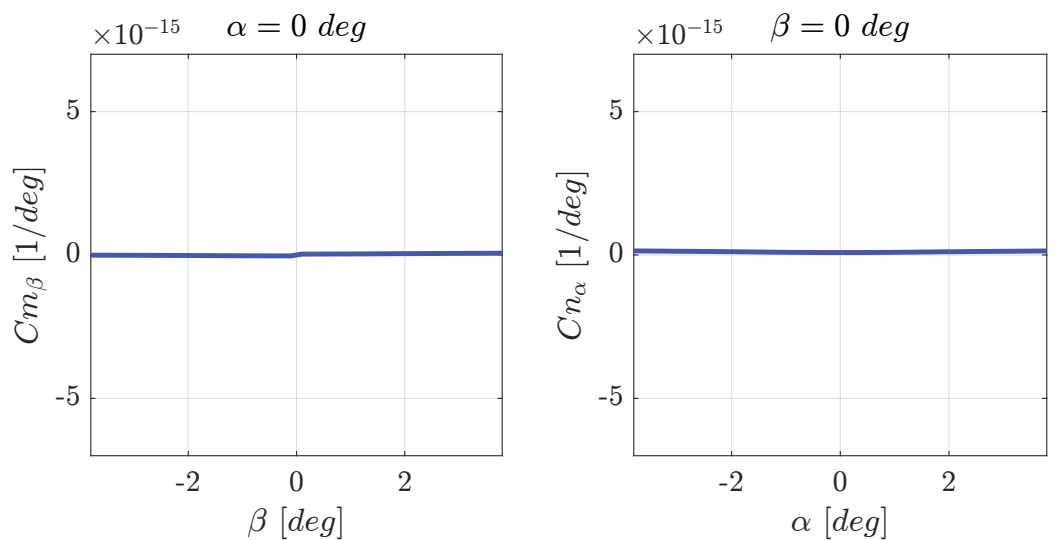

Figure 4. Cross-derivatives of the aerodynamic pitching and yawing moment of a four-finned rocket for changing values of the aerodynamic angles.

2.1.2. Three-Finned Rocket

Rockets with three fins exhibit significantly different behavior in terms of symmetry with respect to the selection of the reference frame where the perturbation is taking place (which is reflected by a different value of angle ϕ). A configuration featuring three fins

at a mutual angle of 120° is considered in this paragraph. As can be seen from Figure 5, considering the longitudinal static stability, C_N is null at ϕ equal to 85° or 275°, yielding asymptotes in the static margin, whereas considering the directional stability, C_Y is null at ϕ equal to 0° or 180°. Therefore, it can be observed that the classical static margins do not display a periodic pattern every 120°, as would be expected from the configuration of the tail.
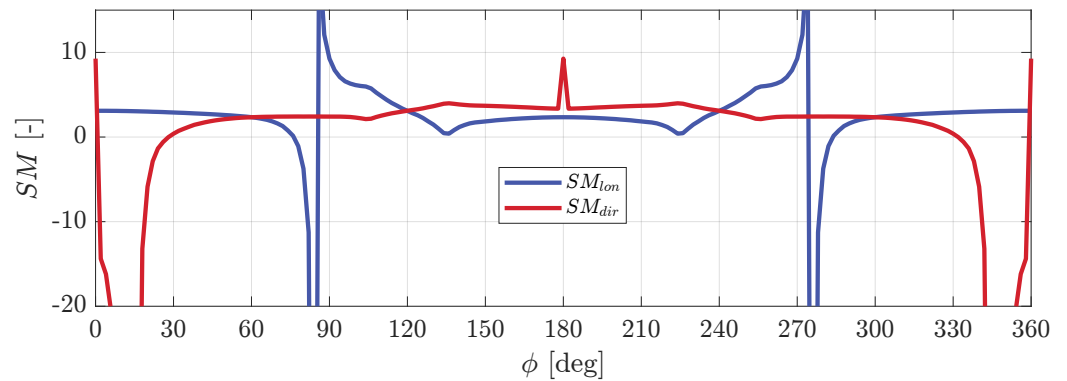

Figure 5. Longitudinal and directional static margins as functions of the aerodynamic roll angle ϕ for a three-finned rocket.

Furthermore, for this rocket configuration, the effect of the choice of the body reference system influences the static stability margins according to the results reported in Table 2. Given a flight condition, the static margin shall uniquely determine the static stability of the rocket without depending on the considered reference frame, as was the case for the four-finned rocket scenario (see Section 2.1.1). Conversely, from Table 2, the same flight condition is predicted as either stable or unstable depending only on the orientation of the body frame, rotated to be aligned with the three fins respectively, while preserving the longitudinal body axis.

Table 2. Longitudinal and directional static margin at $\alpha_{tot} = 15°$ with respect to different reference frames (reflected by different values of ϕ), each with the z^b axis aligned with respect to a different fin in a three-finned configuration.

Reference Frame	$\mathbf{SM_{lon}}$	$\mathbf{SM_{dir}}$	$\boldsymbol{\phi}$
$\mathcal{RF}_1$	3.04	-67.45	16°
$\mathcal{RF}_2$	0.40	3.99	136°
$\mathcal{RF}_3$	5.97	2.12	256°

Comparing Figure 6 to Figure 4 for the four-finned configuration, it can be seen that for a three-finned configuration the cross-derivative $C_{m_{CG_\beta}}$ cannot be neglected. Correspondingly, in this configuration, the two static margins are coupled and, as a consequence, they fail to accurately predict whether a certain missile layout is actually stable or unstable in a certain flight condition.
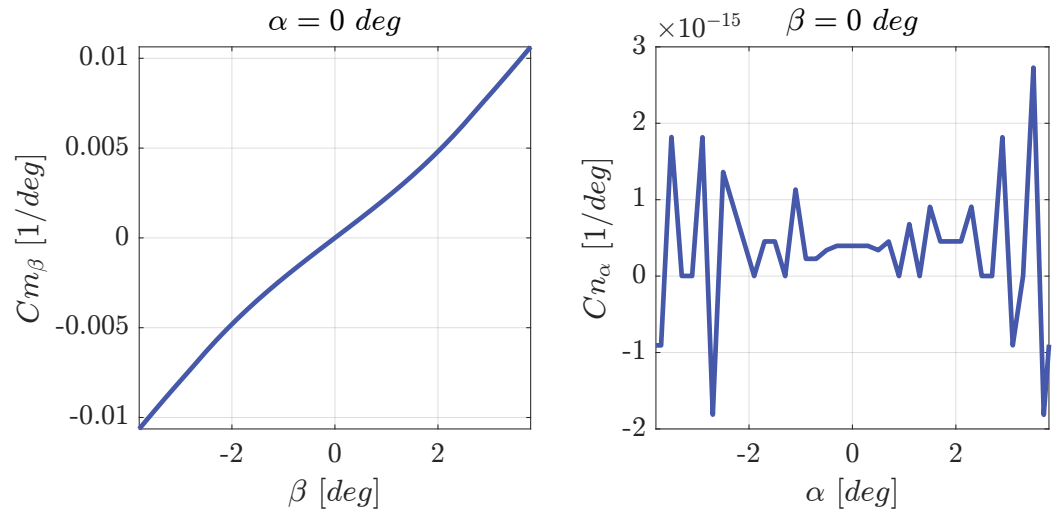
Figure 6. Cross-derivatives of the aerodynamic pitching and yawing moment of a three-finned rocket for changing values of the aerodynamic angles.

3. Compounded Static Stability Index

Originally designed for winged aircraft, the classical formulation of static stability has limitations when applied to axial-symmetric bodies with at least three fins disposed in a radial fashion, such as the sounding rockets of interest. To address these limitations, a single static margin is proposed here, rather than the two static margins currently in use, as shown in Section 2.

To explain the definition of this static margin, consider the usual definition of a body reference frame, as proposed in Figure 1. For simplicity, assume that the missile (or aircraft) is flying with a velocity vector aligned with x^B. Suppose now a perturbation is introduced in the direction of the velocity vector, such that a change in α_{tot}, defined in Figure 2, captures the overall intensity of the perturbation. Considering the front body plane of the aircraft, normal to x^B, it is possible to define a single plane so as to fully contain the perturbed velocity vector, while being normal to the front plane. This plane is here defined as the α_{tot} plane. For example, in Figure 7 the front body plane normal to x^B is shown with the corresponding cross-section of an example three-finned missile. The dashed line marks the plane normal to the front body plane and containing the velocity vector, i.e., the α_{tot} plane.
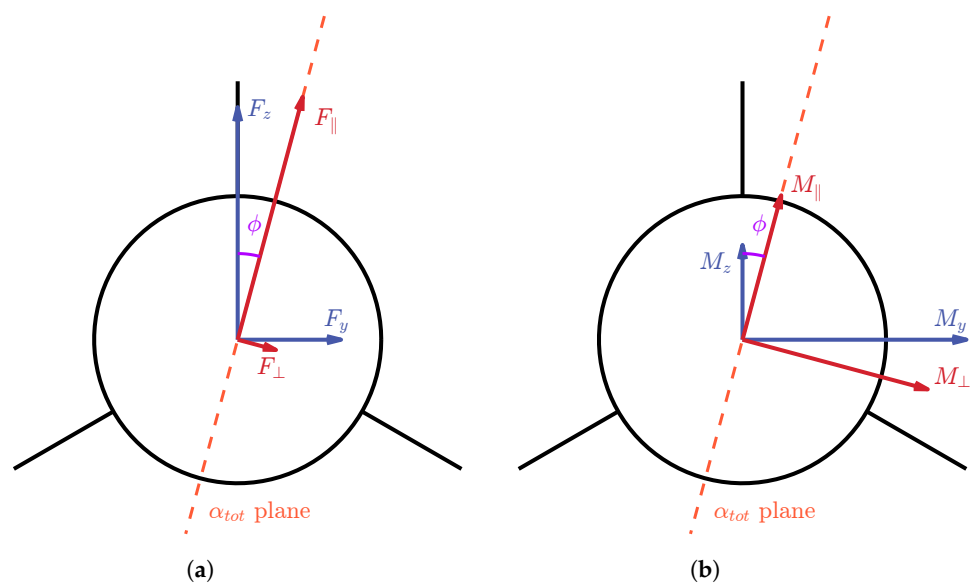

(**a**)

(**b**)

Figure 7. (**a**) Rotated forces; (**b**) rotated moments.

Furthermore, the two plots on Figure 7 show the decomposition of the aerodynamic force and moments ensuing from a velocity vector misaligned with respect to x^B, both with respect to the body reference axes (blue) and to a rotated reference (red). The latter, indicated as $(\cdot)^R$, shares the first axis with the original body reference so that $x^B \equiv x^R$, whereas axes y^R and z^R are defined in the α_{tot} plane and normal to it, respectively. This can be equivalently described by defining the new $(\cdot)^R$ reference as rotated by an angle ϕ around x^B with respect to the original body reference.

Analytically, it is possible to define the planar rotation through which the original and rotated body references are connected as

$$\underline{\underline{R}} = \begin{bmatrix} \cos\phi & -\sin\phi \\ \sin\phi & \cos\phi \end{bmatrix}, \tag{5}$$

whereas the application of this rotation to the original force and moment components in the frontal plane produces the rotated components here defined as

$$\begin{bmatrix} C_Y^R \\ C_N^R \\ C_{m_{CG}}^R \\ C_{n_{CG}}^R \end{bmatrix} = \begin{bmatrix} \underline{\underline{R}} & \underline{\underline{0}} \\ \underline{\underline{0}} & \underline{\underline{R}} \end{bmatrix} \cdot \begin{bmatrix} C_Y \\ C_N \\ C_{m_{CG}} \\ C_{n_{CG}} \end{bmatrix}. \tag{6}$$

According to these definitions, it is possible to introduce a compounded value of the static stability margin as

$$SM_{comp} = \frac{C_{m_{CG}}^R}{C_N^R}, \tag{7}$$

which is representative of the static stability of the system irrespective of the actual direction of the velocity vector perturbation. By substitution of the respective definitions in Equation (7), the explicit expression of the compounded static margin is obtained as

$$SM_{comp} = \frac{C_{m_{CG}} \cos\phi - C_{n_{CG}} \sin\phi}{C_Y \sin\phi + C_N \cos\phi}. \tag{8}$$

*3.1. Assessing Static Stability via the Compounded Static Margin*

While the newly introduced compounded static margin is capable of overcoming the limits of a static stability assessment based on the longitudinal and directional stability for an axial symmetric body (as will be shown in the next Section 4), its ability to describe the level of static stability in a typical winged configuration is worse than that of the classical stability indexes currently employed.

In order to highlight the effectiveness and limits of the compounded index of static stability, an investigation is presented for four different body configurations. These configurations are chosen specifically to highlight that the more a body is able to respond to a perturbation in any direction, the more relevant the compounded margin becomes. This conceptual analysis was carried out with the help of numerical computations, employing the code `Tucan OpenVogel` [14], a software based on a vortex lattice method to estimate the aerodynamic coefficients of classic geometries consistent with all the hypotheses of potential flow theory.

The focus in the analysis is on understanding the existing correlation between the aerodynamic force and moment components associated with an assigned direction of the velocity vector. The conceptual test case scenarios consist of bi-dimensional half-wings with symmetric airfoils, characterized by the geometric parameters listed in Table 3 and defined in Figure 8. The so-defined lifting surface is arranged to produce different configurations.

Table 3. Geometry data of the reference lifting surface adopted in the analysis.

	Value	Unit
Root chord	3	m
Tip chord	1	m
Length (half-span)	5	m
Sweep-back	35	deg
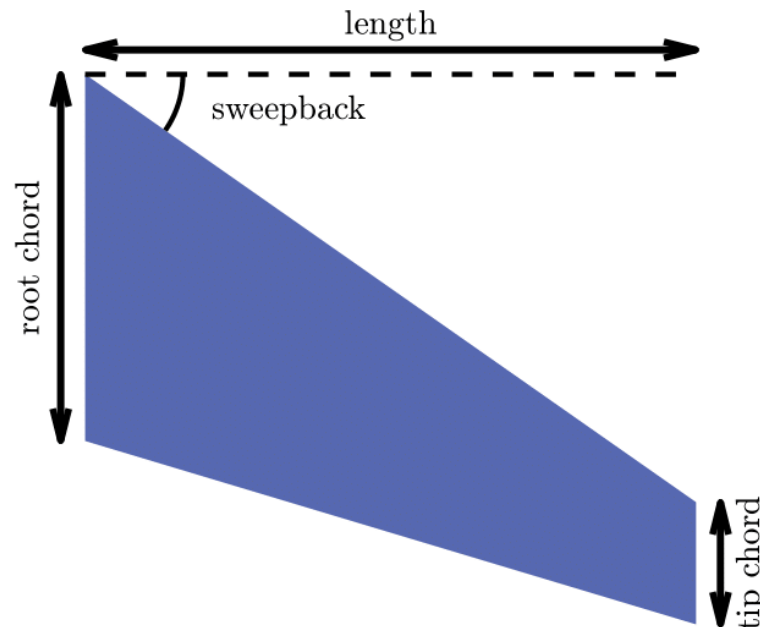
Figure 8. Description of parameters in Table 3.

The four considered configurations can be described as follows:

1. A standard wing with no dihedral angle (Figure 9a).
2. A wing with a dihedral angle of 20° (Figure 9b).
3. A wing with a dihedral angle of −20° (Figure 9c).
4. A set of fins composed of three fins disposed with an angular displacement of 120° between each other (Figure 9d).

The results presented in the following are obtained considering four test cases for each geometry, with values of the sideslip angle $\beta = 0°, 2°, 6°, 8°$, for a total of 16 simulations. The maximum angle of 8° is chosen to safely fall within the range of application of the model of potential flow on which the software is based. The intensity of the velocity vector was set to 50 m/s and the angle of attack $\alpha = 2°$.

Figure 10 shows the results of the analysis, portraying in each plot the outcome of the four experiments carried out on a single configuration. In particular, the plot shows the components of the velocity (red), aerodynamic force (black), and moment (blue) vector lying on the plane normal to x^B.

The 0° dihedral layout simulations show that the directions of the force and moment are invariant with respect to the velocity direction. Actually, for this flying wing configuration, most of the aerodynamic force developed lies parallel to the plane of the airfoils (i.e., $x^B z^B$), whereas the component not belonging to that plane is comparatively negligible. Therefore, such aerodynamic force can only be effective in counteracting a perturbation on α, which is obtained through a corresponding pitching moment. Conversely, the flying wing is not capable of counteracting a perturbation on β (and as a consequence, such an aircraft is not statically stable in a directional sense, as known).
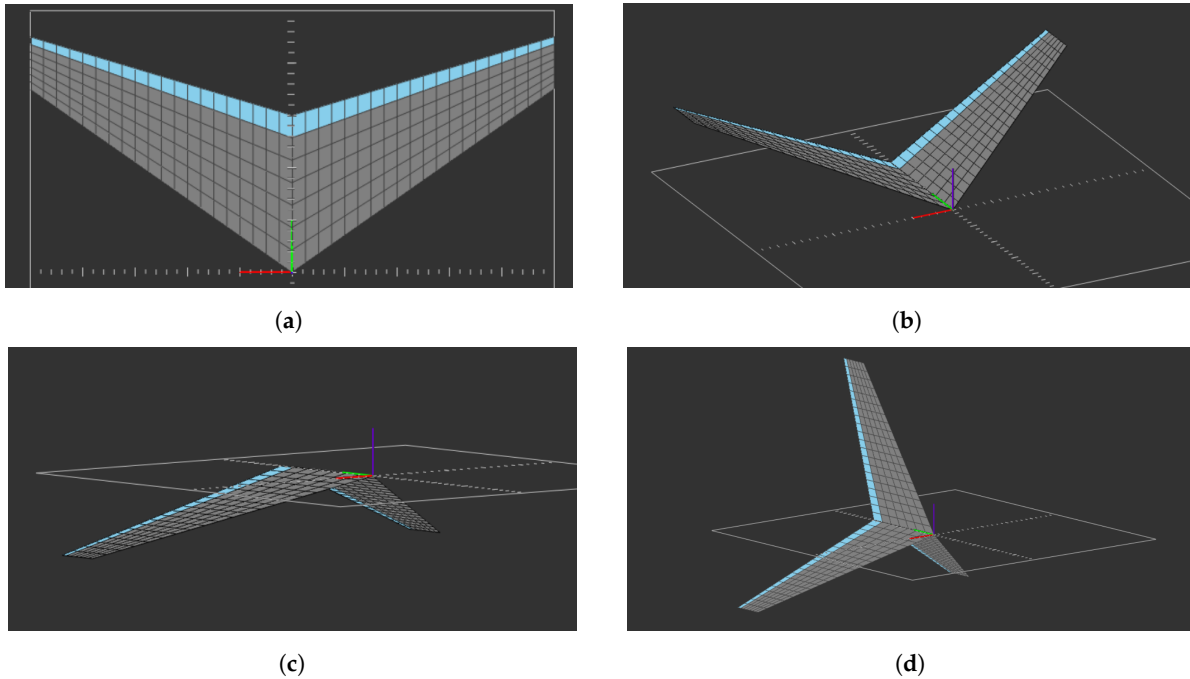
Figure 9. The considered layouts, visualized within `Tucan OpenVogel`: (**a**) no dihedral wing, (**b**) +20° dihedral wing, (**c**) −20° dihedral wing, and (**d**) set of three fins.
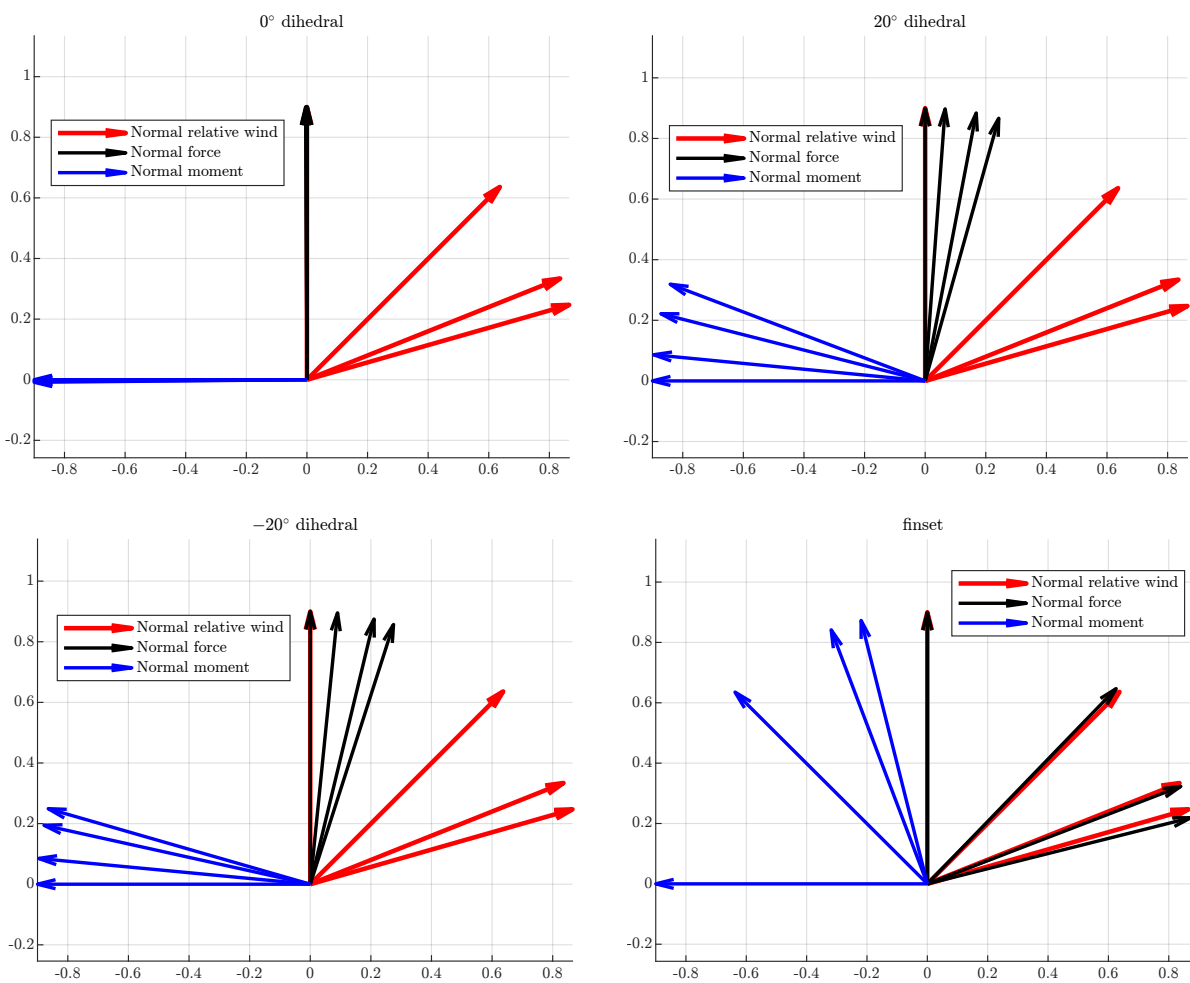

Figure 10. Normal components of the velocity (red), force (black), and moment (blue).

On the other hand, for higher absolute dihedral values (i.e., $+/-20°$), the directions taken by the normal components are correlated with that of the velocity vector.

Finally, for the set of fins, which is of particular relevance since it resembles the fin of a three-finned sounding rocket, a strong coupling with the direction of the velocity vector is similarly obtained.

In order to quantify the ability of a compounded stability index alone to describe the static stability of a system, it is possible to introduce the following parameter e, which is based on the evaluation of the angle Δ defined graphically in Figure 11, and analytically as

$$e = \left| \frac{\frac{\pi}{2} - \Delta}{\frac{\pi}{2}} \right| \cdot 100. \tag{9}$$

Inspecting Figure 10 and analyzing the value of the parameter e, it is possible to note that it captures the level of correlation between the normal component of the relative wind velocity and that of the normal force.
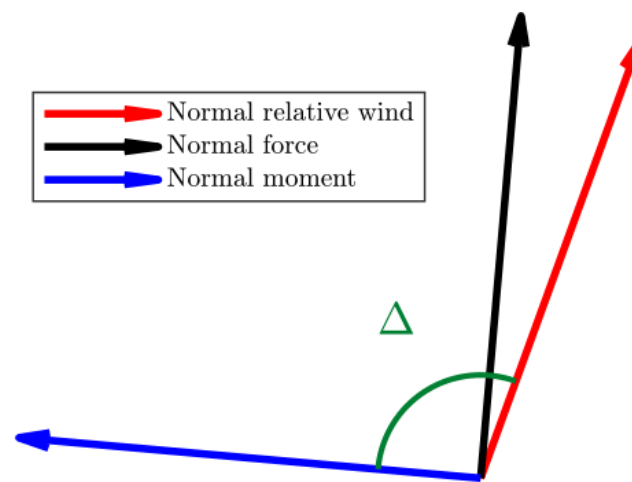

Figure 11. Definition of angle Δ.

In particular, the lower the value of e, the better the correlation. Correspondingly, the significance of the compounded static stability index is increased for lower values of e, meaning that the level of static stability can be employed to better describe the overall (i.e., compounded) level of static stability of the system if the reaction to a perturbation is such as to keep e lower. For example, for the null-dihedral flying wing, the value of e is comparatively high, yielding an inaccurate description of the level of static stability via the compound index, whereas for the set of fins, the parameter e keeps a lower value, and in this case, the compound index of static stability is more descriptive than the two classical indexes for longitudinal and directional stability.

To physically explain this effect, it can be said that the compounded static stability index can be employed to study the static stability of an aircraft when the angle Δ between the normal component of the total aerodynamic moment and the normal component of the relative wind is sufficiently close to $\Delta = \frac{\pi}{2}$, for every combination of α and β (which is captured by a corresponding value of α_{tot}) within a reasonable range. This result is conveniently shown in quantitative terms in Figure 12, where the parameter T has been defined as a function of e only, as

$$T = 100 - e = 100 - \left| \frac{\frac{\pi}{2} - \Delta}{\frac{\pi}{2}} \right| \% \tag{10}$$

According to its definition, this parameter shall take a higher value for a more reduced level of parameter e. The plot in Figure 12, referring to the trials at several values of the angle ϕ considered in the test at hand (which are obtained for the assigned α and β

values, where, in particular, only the latter has been changed, as said), shows that for the flying wing at null dihedral, the compounded stability index is descriptive only for $\phi = 0$, i.e., when this index is the same as that for the longitudinal static stability. In all other cases, the compound index is poorly descriptive of the level of static stability for this configuration. Substantially similar results are obtained for the flying wing with a positive or negative dihedral. Conversely, for the set of fins, for whatever ϕ, the compounded stability index remains descriptive of the static stability level, whereas the two classical indexes are not, as pointed out in Section 1 as a problem statement.
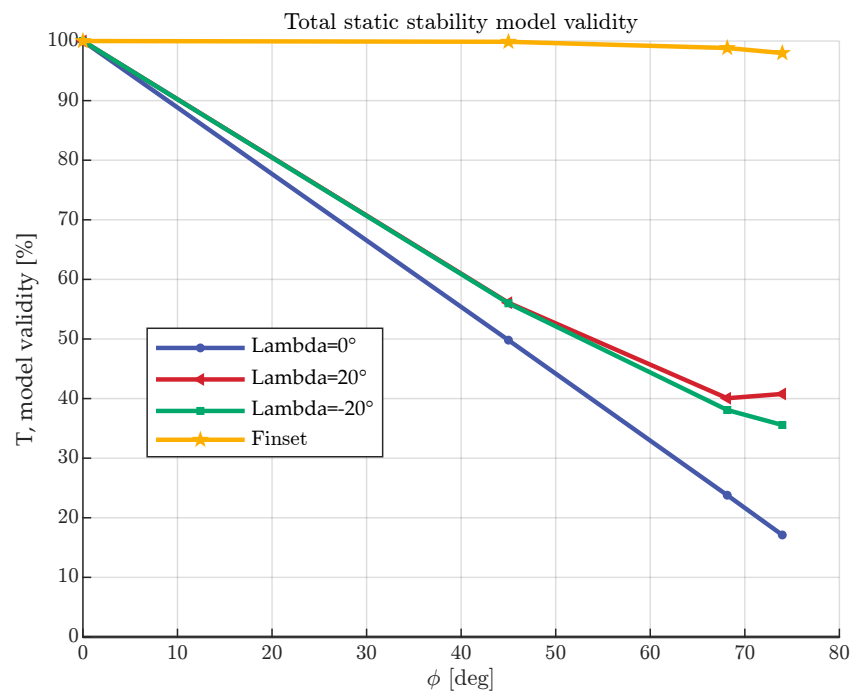

Figure 12. Parameter T as a function of the aerodynamic roll angle.

4. Analysis of Compounded Stability of a Realistic Sounding Rocket Configuration

4.1. Three-Finned Configuration

The configuration of a missile with a tail assembly composed of three fins placed at $120°$ from one another is of special relevance in sounding rocket applications. In Section 3.1, it was shown that a three fins assembly can be effectively described in terms of static stability through the compounded index introduced earlier in this text. A missile featuring that tail assembly is generally constituted by an axial-symmetric body and the tail itself. For an axial-symmetric body, like the one in Figure 13, it is intuitive to choose a reference frame that contains the velocity vector in its $x^B z^B$ plane. This plane coincides with the α_{tot} plane defined previously, so that evaluating the longitudinal static margin in a reference where the $x^B z^B$ plane is equal to the α_{tot} plane allows to completely characterize the static response of the body. Therefore, for an axial-symmetric body also, it can be expected that the compounded static margin will be totally descriptive of the static stability level of the system.

In order to show this in a practical case, the configuration and data for the *Gemini* [15] sounding rocket are employed. Computations of the aerodynamic coefficients on this configuration were carried out in both `Missile DATCOM 97` and `ANSYS Fluent` [16], showing good correlation (see Appendix A). A testing condition with a velocity of 32 m/s, $\alpha_{tot} = 16°$ and $\rho = 1.225$ kg/m^3 was considered. The rocket was set at several rotated conditions, so as to produce values of ϕ ranging between $0°$ and $360°$. These values come directly from the aerodynamic design process of *Gemini*, as is thoroughly explained in Section 5. Figure 14 describes the output of the analysis in terms of the components of the force and moment coefficients (normalized on their respective maxima to ease the comparison of

trends), in the original body reference (attached to the missile, top plots) and in the rotated $(\cdot)^R$ reference (bottom plots), respectively.
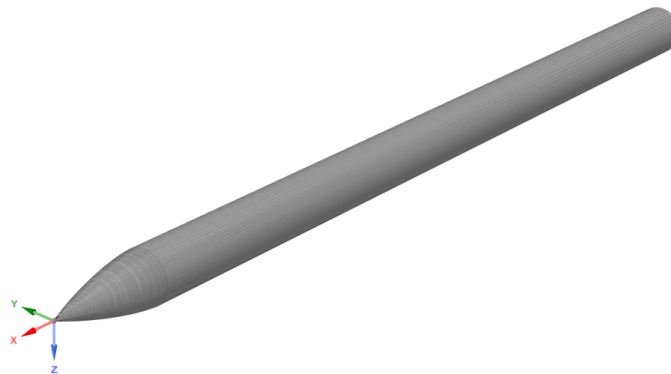

Figure 13. Axial symmetric slender body of revolution.

In Figure 14c,d, it can be seen how C_N and $C_{m_{CG}}$ show the same pattern since they are related to the longitudinal domain of the missile, while C_Y, $C_{l_{CG}}$ (the rolling moment coefficient) and $C_{n_{CG}}$, related to the lateral directional behavior, follow a different trend, uncorrelated from that of the other quantities. The overall force coefficient C_A instead keeps a constant value in each flight condition, which is in accordance with the fact that the speed and the total angle of attack remain constant.

The response along the longitudinal axis of the rotated frame is the one directly involved in statically contrasting the perturbation itself (tending to reduce the value of α_{tot}).

Figure 15 shows a direct comparison of the classical longitudinal and directional static margins, as well as the compounded margin, for the same missile model and testing conditions. It can be seen from this plot that the compounded static margin produces a clearer and more complete assessment of the level of static stability of the platform, which, as expected, is far less variable for different ϕ than is suggested by the classical indexes, which appear harder to interpret and are largely misleading in this case.

It can be observed that, as Figure 15 shows, the compound stability index converges to the classical longitudinal index when ϕ tends to $0°$ or $180°$, and to the directional index when ϕ goes to $90°$.

4.2. More Geometries

The compounded stability formulation presented in this paper allows to accurately assess the level of static stability for a body of revolution with more than two fins. To show this, an analysis similar to that just presented for a three-finned missile was performed for several different configurations.

In particular, a set of rocket models was created by varying the total L/D ratio, the geometry of the fins, and their number, according to Table 4.

All the permutations were evaluated, discarding those producing extreme geometries, which are of no interest for practical applications.

Each valid model was tested in the flight conditions reported in Table 5.

The T index was computed for all the considered flight conditions and geometries. The results are presented in the histogram in Figure 16. This shows the frequency at which a certain value of T appears within the considered sample space.

The generally high value of the T index, combined with the representativeness of the sample, shows that this type of flying craft is generally well−described in terms of static stability by employing the compounded stability index introduced in this text.
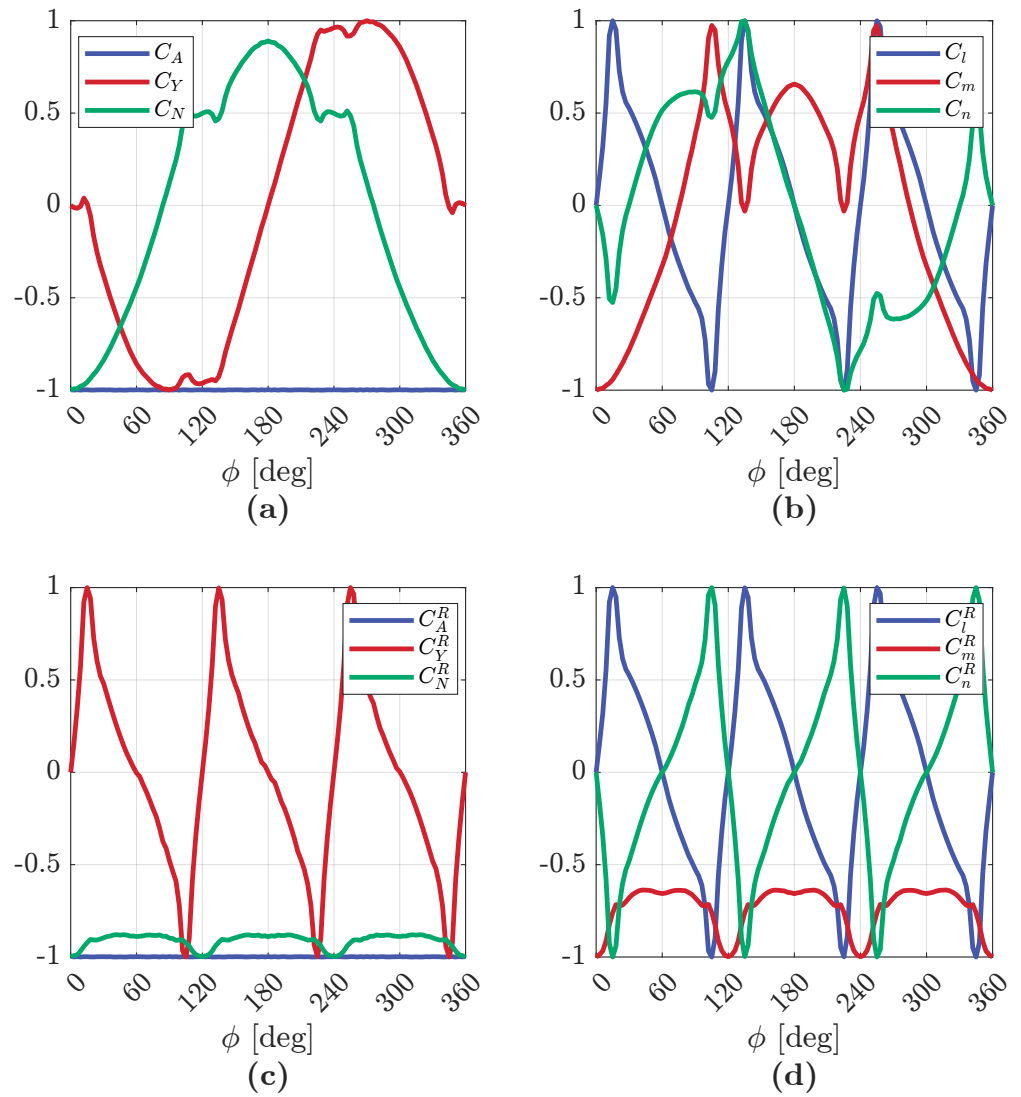
Figure 14. Data at v = 32 m/s and α_{tot} = 16 deg: (**a**) force coefficients; (**b**) moment coefficient; (**c**) force coefficients rotated; (**d**) moment coefficients rotated.
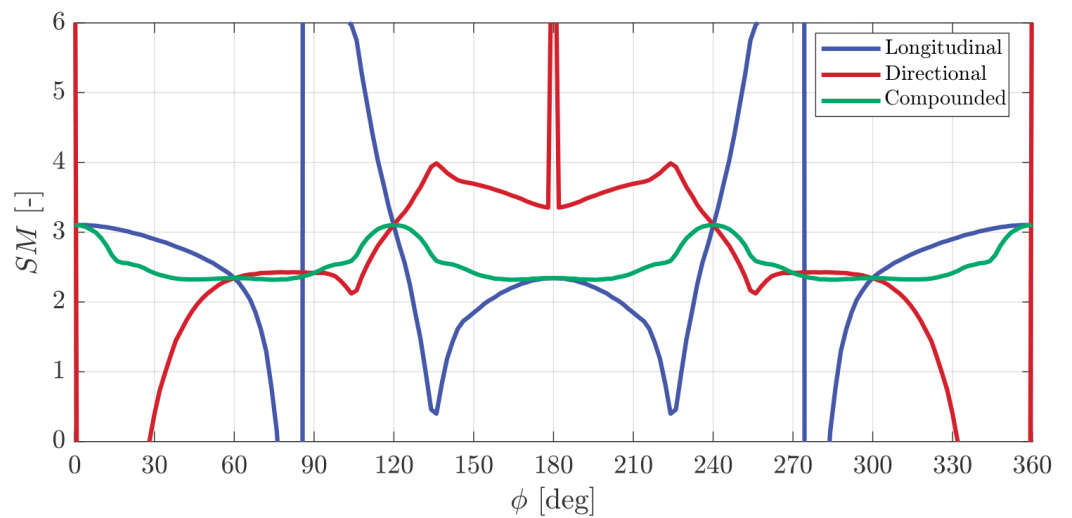

Figure 15. Comparison between the classical and the compounded static margins for the three-finned missile.

Table 4. Rocket geometries for the analysis of the compound stability index validity.

Parameter	Values	Unit
Root chord	0.2, 0.4, 0.6	m
Free chord	0.1, 0.2, 0.3	m
Fin height	0.1, 0.2, 0.3	m
Fins number	3, 4, 5	−
Sweep−back length	0.1, 0.2	m
Fuselage diameter	0.1, 0.40, 0.60	m
Center body length	2, 3, 4	m

Table 5. Flight conditions considered for testing the validity of the compound stability index.

Parameter	Values	Unit
Angle of attack	−20, −16, −12, −8, −4, −1, 0, 1, 4, 8, 12, 16, 20	deg
Sideslip angle	−20, −16, −12, −8, −4, −1, 0, 1, 4, 8, 12, 16, 20	deg
Mach number	0.1, 0.3, 0.5	−
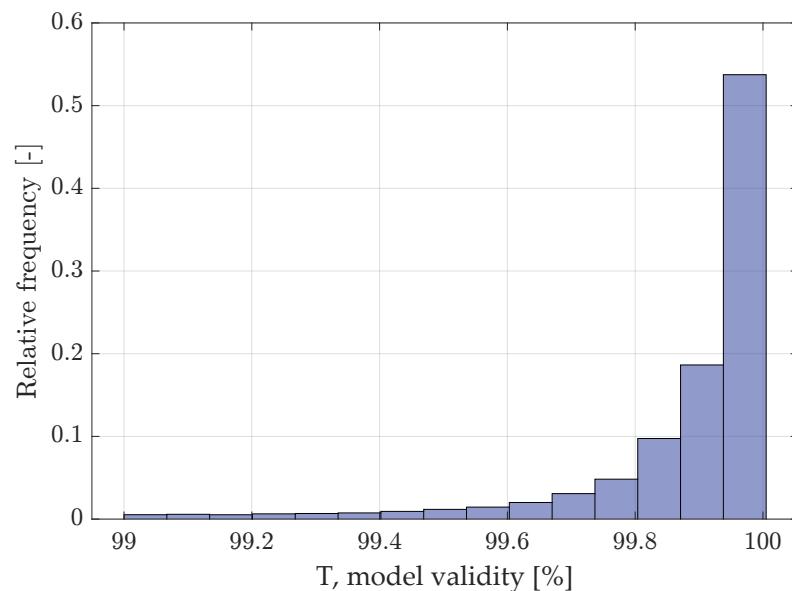
Figure 16. Distribution of T index, considering all testing conditions and configurations in Tables 4 and 5.

5. Field Case Study: the *Gemini* Sounding Rocket

The method presented in this article was applied in the design process for the *Gemini* rocket built by Skyward Experimental Rocketry [15], the first-ever SRAD (student-researched and developed) hybrid−powered rocket launched in Italy. The launch took place in Roccaraso on 19 September 2023. The rocket reached an altitude of 1350 m AGL and was successfully recovered. Two representative pictures of the flight are shown in Figure 17, while its geometry data and flight quantities are reported in Tables 6 and 7, respectively. The launch occurred with a crosswind of 3 m/s at ground level, increasing to 14 m/s at the apogee altitude. No stability anomalies were observed during the flight, which was, therefore, considered nominal in terms of flight dynamics.
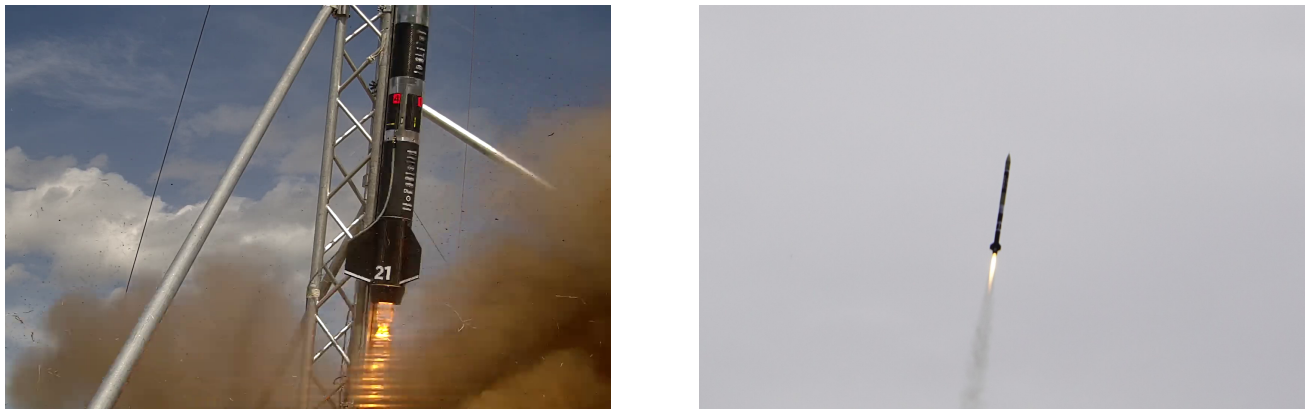
(**a**)

(**b**)

Figure 17. (**a**) *Gemini* lift-off from the launch rail; (**b**) *Gemini* airborne during the powered ascent phase.

Table 6. *Gemini* rocket geometry data.

Section	Feature	Value	Unit
Nosecone	Length	0.32	m
	Shape	Von Karman	−
Center body	Length	2.89	m
	Diameter	0.15	m
Fins	Root chord	0.30	m
	Free chord	0.14	m
	Span	0.11	m
	Number	3	−
	Sweepback length	0.13	m
Boat tail	Length	0.07	m
	Final diameter	0.122	m

Table 7. *Gemini* rocket flight data.

Parameter	Value	Unit
Apogee	1350	m
Time to Apogee	17.5	s
Max Speed	150	m/s
Max Mach	0.45	−
Max Thrust	1800	N
Burning Time	4	s

The aerodynamic design of *Gemini* was aimed at maximizing the rocket apogee while maintaining the worst-case static margin over an a priori specified limit of $SM = 2.0$ in this case. The sizing of the tail fins was carried out specifically for this purpose.

It was observed that the worst-case condition in terms of static stability occurs at the launch rail exit when the rocket is fully airborne at its slowest speed and its center of mass is simultaneously at the lowest (i.e., most backward) possible position. The results presented here from the static stability analysis are, therefore, from that phase.

At a design level, in order to ensure a sufficient level of static stability for the finalized aerodynamic shape even in the worst−case scenario, the static margin was calculated for a set of realistic yet conservative meteorological conditions, determined by studying the launch location historical weather data.

This analysis resulted in the selection of a wind magnitude ranging from 0 to 9 m/s, with no restrictions on direction. The static margin was evaluated knowing the speed and direction of both the sounding rocket and wind at the launch rail exit in each flight condition, thus allowing computation of the flight Mach number as well as the total angle

of attack α_{tot} and the aerodynamic roll angle ϕ. Figure 18 shows the output of this analysis through a comparison of the output of the compounded method and the classical one, based on the decoupled longitudinal and directional static stability indexes.
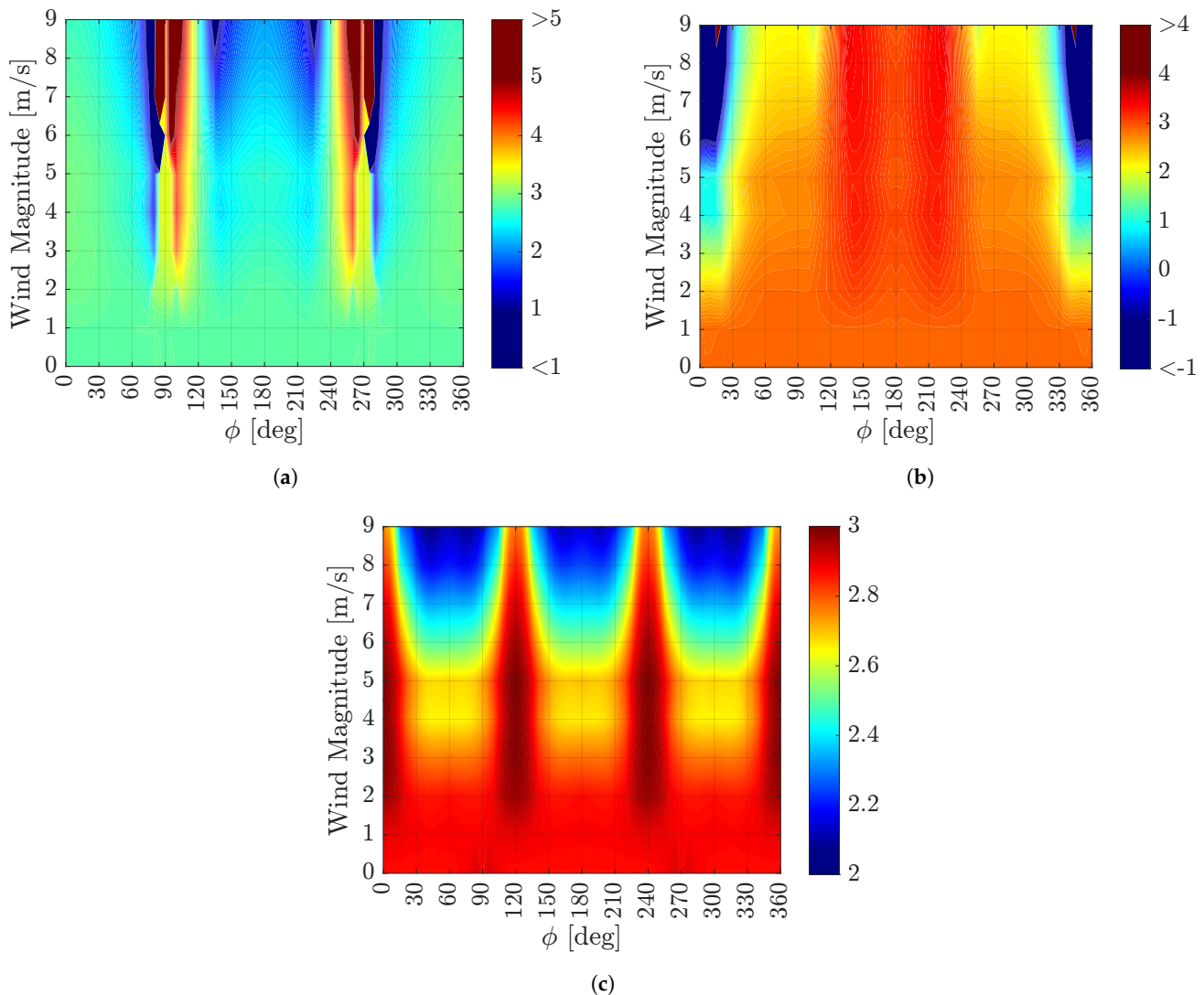

(a)

(b)

(c)

Figure 18. Longitudinal (**a**), directional (**b**), and compounded (**c**) static margin behavior as functions of the wind intensity and direction.

As can be seen, the output of the classical approach (standard stability indices) feature significant discontinuities, proving unreliable in the correct assessment of the static stability of the rocket, which was proved practically in flight.

In particular, asymptotes arise above a wind intensity of 2 m/s on both classical static margin indices. In Figure 18a, the longitudinal static margin shows asymptotes around $\phi = 90°$ and $\phi = 270°$, whereas in Figure 18b, the directional static margin shows an asymptote around $\phi = 0°$.

In practical terms, since during the design process the minimum value of the static margin index needs to be checked to be over the desired value (as previously pointed out), the longitudinal and directional indexes were discarded as possible measures of performance due to their non-significant behavior and reading.

On the other hand, the compounded method retains stable behavior in the whole envelope of wind direction and intensity, and consequently better represents the intensity of the static response of the rocket to a perturbation. Accordingly, the compounded static

margin was chosen to be the best static stability index for the design process of the *Gemini* sounding rocket.

The ensuing design proved faultless from the standpoint of static stability, confirming the suitability of the proposed compounded stability index for the design of this type of machine.

6. Conclusions

The present paper deals with the specific issues connected with the analysis of the static stability of sounding rockets. The typical design configuration of the latter, basically featuring an axial-symmetric main body and a set of fins, often produces results that are difficult to interpret when it comes to judging the level of static stability of the system through classical methods. In particular, the latter separately analyze the longitudinal and directional static stability. In this paper, it was shown how the results of that analysis, especially on three-finned tail configurations, are rather difficult to interpret, poor in generality, even for a specific missile sizing, and potentially misleading, i.e., in particular, predicting static stability issues when these do not actually appear in practice.

In order to overcome these limitations of standard static stability analyses, a compounded static stability index and criterion were introduced, based conceptually on a smart selection of the plane where the static stability analysis is carried out. After introducing this stability analysis method both conceptually and analytically, its inherent advantages and limits were thoroughly assessed by practically applying it to several geometries and testing conditions. By selecting some extreme configurations for preliminary testing in a virtual environment, the physics behind the proposed criterion were analyzed in-depth, highlighting its limits. For realistic missile configurations, the method appears generally to be promising, and extensive testing on several geometries confirms its general applicability to the static stability analysis of typical sounding rocket geometries, with results which are more complete and easier to interpret with respect to those obtained from a classical approach.

Then the newly introduced methodology was applied to the design and aerodynamic sizing of the sounding rocket *Gemini*, which flew successfully in September 2023. The design of that sounding rocket was carried out in practice employing predictions of the static stability level defined through the compounded index introduced here. In contrast to the predictions of the classical stability assessment methods (i.e., a potentially highly troublesome static stability level), the compounded method forecast a trouble-free static response, which was verified in practice when the rocket was actually launched.

Further investigations of the newly introduced method, which proved very promising in field application also, will involve its suitability in supersonic flight regimes, whereas the current analyses considered subsonic flight as the case of interest.

Appendix A

Appendix A.1

Each result in this paper was validated by comparing `Missile DATCOM 97` [12] and CFD simulations in `ANSYS Fluent 2022 R1` [16]. The validation was carried out first in terms of the aerodynamic coefficients, subsequently computing the corresponding static margins.

The coefficients involved in the lateral and directional motions show a good correlation between the `Missile DATCOM 97` and CFD simulations, as evidenced by the plots in Figures A1 and A2.
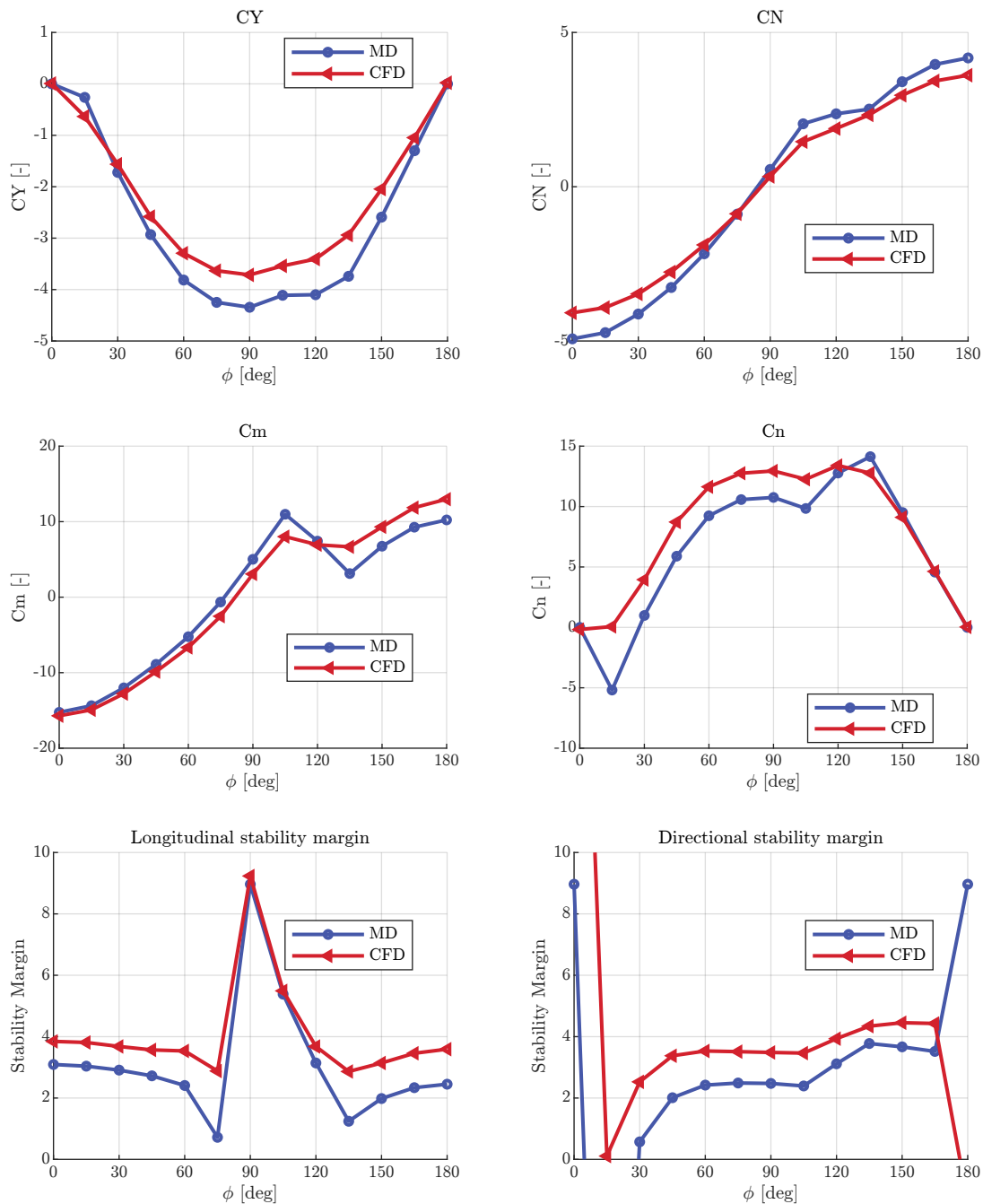

Figure A1. Comparison between the values of C_Y, C_N, $C_{m_{CG}}$, $C_{n_{CG}}$ and the longitudinal and directional stability margins SM_{lon} and SM_{dir} for the reference three-finned configuration, obtained from `Missile DATCOM 97` and CFD simulations in `ANSYS Fluent 2022 R1`.
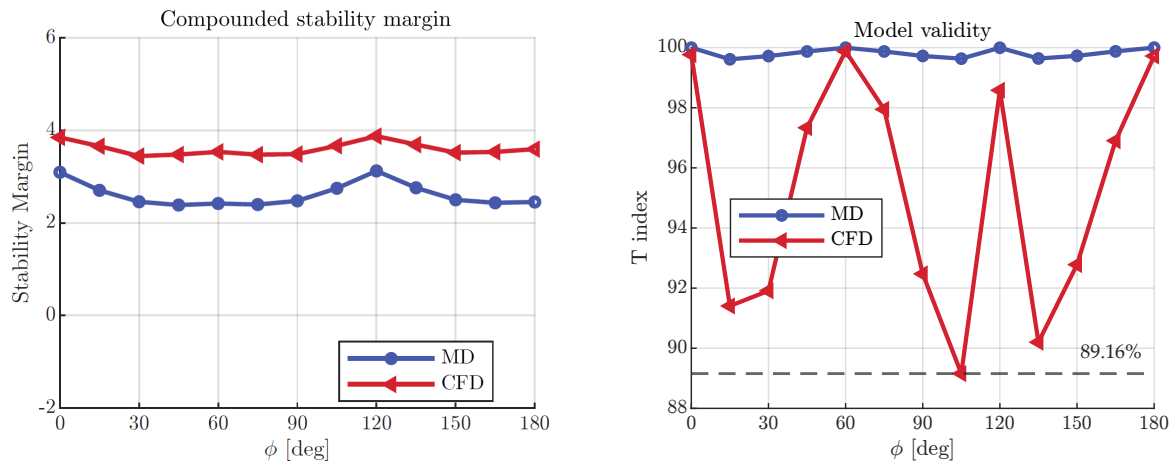
Figure A2. Comparison between the values of the compound static margin and the *T* index for the reference three-finned configuration, obtained from `Missile DATCOM 97` and CFD simulations in `ANSYS Fluent 2022 R1`.

Appendix A.2

All CFD simulations were computed in steady−state. The fluid domain is bullet-shaped because different directions of the relative wind are needed. The mesh is a poly-hexcore mesh [17] computed through the mesher available within the code suite, and counts 2.8 million elements. This elements count was chosen because it is above the mesh independence value of 2.5 million, stated through a parallel mesh independence campaign. All simulations were performed at Mach number $M = 0.1$ at an air density of $\rho = 1.225\ \text{kg/m}^3$; therefore, a set of incompressible settings are chosen.

The turbulence model employed is the standard $k - \omega$ SST, widely adopted in cases like this.

The boundary layer is composed of 20 cells, where the first layer height is $5 \cdot 10^{-6}$ m, chosen after a few iterations to achieve a maximum value of $y^+ = 1$ on the walls of the rocket model.
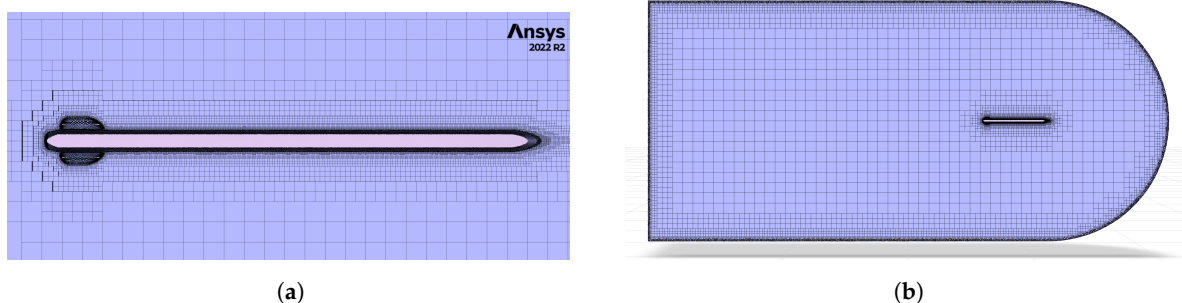

(**a**)

(**b**)

Figure A3. Fluid domain hexahedral dominant mesh. (**a**) Polyhedral elements near the body; (**b**) hexahedral elements sufficiently far from it.

References

1. Cook, M.V. *Flight Dynamics Principles*, 2nd ed.; Elsevier Ltd.: Amsterdam, The Netherlands, 2007; pp. 33–71.
2. Nelson, R.C. *Flight Stability and Automatic Control*, 2nd ed.; WCB/McGraw Hill: New York, NY, USA, 1998; pp. 40–44.
3. Pamadi, B.N. *Performance, Stability, Dynamics, and Control of Airplanes*, 2nd ed.; American Institute of Aeronautics and Astronautics: Reston, VA, USA, 2000; pp. 165–319
4. Fleeman, E.L. *Tactical Missile Design*, 1st ed.; American Institute of Aeronautics and Astronautics: Reston, VA, USA, 2001; pp. 51–53.
5. Ferris, J.C. *Static Stability Investigation of a Single-Stage Sounding Rockets at Mach Numbers from 0.60 to 1.20*; NASA Technical Report TN D-4013; Langley Research Center: Langley Station, VA, USA, 1965.

6. Niskanen, S. OpenRocket Technical Documentation: 2013. Available online: https://github.com/openrocket/openrocket/releases/download/OpenRocket_technical_documentation-v13.05/OpenRocket_technical_documentation-v13.05.pdf (accessed on 30 October 2023).

7. Vallini, L. Static and Dynamic Analysis of the Aerodynamic Stability and Trajectory Simulation of a Student Sounding Rocket. Master's Thesis, Università di Pisa, Pisa, Italy, 2014. Available online: https://core.ac.uk/download/pdf/79617836.pdf (accessed on 30 October 2023)

8. Barrowman, J.S.; Barrowman, J.A. *Theoretical Prediction of the Center of Pressure*; National Association of Rocketry: Marion, IO, USA, 1966. Available online: https://www.nar.org/wp-content/uploads/2016/01/barrowman_cp_extended_edition.pdf (accessed on 30 October 2023).

9. Blakelock, J.H. *Automatic Control of Aircraft and Missiles*, 2nd ed.; Wiley: New York, NY, USA, 1990; Chapters 1–4.

10. Zarchan, P. *Tactical and Strategic Missile Guidance*, 2nd ed.; American Institute of Aeronautics and Astronautics: Washington, DC, USA, 1994.

11. Langham, T.F.; Washington, E.S. *Missile Motion Sensitivity to Dynamic Stability Derivatives*; Arnold Engineering Development Center, Air Force Systems Command, United States Air Force: Washington, DC, USA, 1980; Volume 80. Available online: https://apps.dtic.mil/sti/tr/pdf/ADA089750.pdf (accessed on 30 October2023).

12. Williams, J.E.; Vukelich, S.R. *The USAF Stability and Control Digital DATCOM*; Users Manual [R]; Usaf Stability & Control Digital Datcom: St. Louis, MN, USA, 1979; Volume I. Available online: https://apps.dtic.mil/sti/citations/ADA344707 (accessed on 30 October 2023).

13. Vukelich, S.R. *Development Feasibility of Missile Datcom*; Flight Dynamics Laboratory, Air Force Wright Aeronautical Laboratories, Air Force Systems Command, United States Air Force: Washington, DC, USA, 1981; Volume 81. Available online: https://apps.dtic.mil/sti/pdfs/ADA127378.pdf (accessed on 30 October 2023).

14. Openvogel Tucan. Available online: https://github.com/OpenVOGEL/Tucan (accessed on 30 October 2023).

15. Skyward Experimental Rocketry. Available online: https://skywarder.eu (accessed on 30 October 2023).

16. Ansys Fluent. Available online: https://www.ansys.com/products/fluids/ansys-fluent (accessed on 30 October 2023).

17. Ansys Fluent Mosaic Meshing. Available online: https://www.ansys.com/products/fluids/ansys-fluent/mosaic-meshing (accessed on 30 October 2023).